Giampiccolo A, Ansell MP, Tobaldi DM and Ball RJ (2016) Synthesis of Co–TiO_2 nanostructured photocatalytic coatings for MDF substrates. *Green Materials*, http://dx.doi.org/10.1680/jgrma.16.00004

Green Materials

Research Article
Received 09/02/2016 Accepted 09/11/2016
Keywords: doping/nanostructures/photocatalysts

ice | science

ICE Publishing: All rights reserved

ice Institution of Civil Engineers publishing

Synthesis of Co–TiO_2 nanostructured photocatalytic coatings for MDF substrates

Andrea Giampiccolo BSc*
PhD student, BRE Centre for Innovative Construction Materials, Department of Architecture and Civil Engineering, University of Bath, Bath, UK

Martin P. Ansell BSc, PhD, FIMMM
Reader in Materials, BRE Centre for Innovative Construction Materials, Department of Architecture and Civil Engineering, University of Bath, Bath, UK

David Maria Tobaldi MSc, PhD
Research Associate, Department of Materials and Ceramic Engineering, Ciceco – Aveiro Institute of Materials, University of Aveiro, Aveiro, Portugal

Richard J. Ball BEng, PhD, FHEA, CSci, CEng, FIMMM
Reader in Materials, BRE Centre for Innovative Construction Materials, Department of Architecture and Civil Engineering, University of Bath, Bath, UK

This paper describes for the first time the development of novel photocatalytic coatings specifically for medium-density fibreboard (MDF) substrates. Anatase nanostructures were manufactured using a sol–gel synthesis route and subsequently heat-treated to form micro-sized agglomerates. In this study titanium dioxide particles were doped with cobalt in order to reduce the band gap and promote photocatalysis in the visible wavelength range. These agglomerates were then bound to MDF using a polyurethane-based binder. The subsequent coatings were tested under white, green and ultraviolet light using ink intelligent photoactive dyes in a gaseous environment and methylene blue indicator in an aqueous environment. Manufactured particles were also compared to the commercially available products P25 and Kronoclean 7000. The physical and chemical properties of the manufactured particles and substrates were evaluated using electron microscopy, X-ray diffraction and Raman spectroscopy. This work demonstrates the performance of photocatalytic coatings applied to MDF.

Notation

A	absorbance
C	concentration of dye
l	path length
ε_λ	molar absorption coefficient

1. Introduction

Increasing awareness of the health risks associated with exterior atmospheric pollutants and volatile organic compounds (VOCs) in the indoor environment is stimulating research aimed at improving air quality. Since Honda and Fujishima[1,2] discovered the photocatalytic properties of titanium dioxide (TiO_2) for water splitting, the application of photocatalytic materials for degrading VOCs has been identified as a promising approach to improving air quality, and research in the field has increased exponentially.[3] The widespread use of titanium dioxide can be attributed to its relatively low ratio of cost to photocatalytic activity and non-toxicity. The band gap of 3·2 eV requires short wavelength ultraviolet (UV) light to activate the photocatalytic properties of titanium dioxide.[4] However, the intensity of UV only accounts for a few per cent of the solar spectrum and is even lower within buildings.[5] This greatly reduces the potential of titanium dioxide to catalyse the oxidation or reduction of harmful compounds to innocuous products such as water or carbon dioxide. The photocatalytic activity of a semiconductor can be enhanced by various methods, including doping with noble metals, transition metals and non-metallic elements.[6] The formation of an additional electronic state in the bandgap will be induced by the introduction of a foreign element into the lattice. This will allow multiple electronic transitions to be initiated by visible light, which improves the photocatalytic efficiency of titanium dioxide.

Titanium dioxide in the form of nanoparticles is finding increasing applications for improving indoor and outdoor air quality.[7–9] A wide range of chemicals, such as inorganic pollutants and VOCs, are emitted by a variety of materials in buildings[10–13] such as furnishings, paints, carpets and air fresheners. The presence of VOCs and other harmful chemicals is a significant contributing factor to 'sick building syndrome',[14] which describes the negative impact a building's environment can have on the life and performance of its inhabitants.

To mitigate against sick building syndrome, the EU-funded project Eco-innovative, Safe and Energy Efficient Wall Panels and Materials for a Healthier Indoor Environment is developing a building panel from eco-compatible materials to improve moisture and temperature control, acoustic isolation and indoor air quality. Titanium dioxide-based photocatalytic materials will make an important contribution to achieving this objective.

This paper describes the synthesis and characterisation of cobalt-doped and undoped titanium dioxide nanoparticle aggregates (NPAs). Synthesised through a sol–gel processing method, these were developed for application to wood substrates. Field emission scanning electron microscopy (FESEM) and standard scanning electron microscopy (SEM), Raman spectroscopy and energy-

***Corresponding author e-mail address:** a.giampiccolo@bath.ac.uk

dispersive X-ray analysis (EDX) techniques were used to characterise the physical and chemical properties of the cobalt (Co)-doped and undoped nanoparticles, thereby allowing comparison with the commercially available nanoparticle products Degussa P25 and Kronoclean 7000.

To use a photocatalytic material effectively, it is necessary to immobilise it on the surface of a substrate. This can present a challenge, as the coating procedure must maintain the photocatalytic activity of the particles and not lead to any adverse consequences, such as the degradation of the surface. In this paper, the authors investigate the performance of a photocatalytic coating specifically developed for application to a medium-density fibreboard (MDF) finished with a melamine formaldehyde-impregnated paper substrate.

MDF is used worldwide for many applications, including building and furniture constructions. It has a number of advantages when compared to natural wood which are mainly associated with its homogeneity and absence of defects such as knots and irregularities. MDF has properties that can be tuned by varying the type of resin, the constitution of the fibres and the manufacturing parameters for the fibreboard.[15–17] For certain applications, this manufacturing flexibility can be a distinct advantage, but the formaldehyde resins (e.g. melamine urea formaldehyde (MUF)) used to bind the wood fibres are responsible for particularly high emission of aldehydes[18] and other VOCs.

2. Experimental methodology

2.1 Sol–gel synthesis of cobalt-doped and undoped titanium dioxide NPAs

Manufacture of titanium dioxide through a sol–gel method is based on the hydrolysis and polymerisation of a metal–organic precursor to form a colloidal suspension.[19,20] In the synthesis, 10 ml of titanium (Ti), tetraisopropoxide (Sigma Aldrich, ≥98%; MM = 284·22; d = 0·96 g/ml) was mixed with 40 ml of 2-propanol (Sigma Aldrich, ≥99·7%; d = 0·785 g/ml) in a round-bottomed flask. That flask, which also acted as the reaction vessel, was positioned above a hotplate/magnetic stirrer (Figure 1) within a fume cupboard. The reaction vessel was placed inside a flat crystalliser dish filled with water, thereby ensuring that the flask was heated evenly at a temperature of 80°C. A separator funnel mounted above the round-bottomed flask was filled with a deionised water solution of cobalt (II) chloride ($CoCl_2$) adjusted to pH of 2 using nitric acid. In the synthesis of undoped titanium dioxide, acidified deionised water was added to the alcoholic solution with the titanium precursor. The acid provided the optimum pH for the hydrolysis reaction. A 7×10^{-4} M solution concentration of cobalt (II) chloride was used to achieve a dopant concentration of 1 at.% in the titanium dioxide lattice.

The 2-propanol and the titanium precursor were maintained at a temperature of 80°C under constant vigorous magnetic stirring for 1 h before the aqueous cobalt chloride solution was allowed to

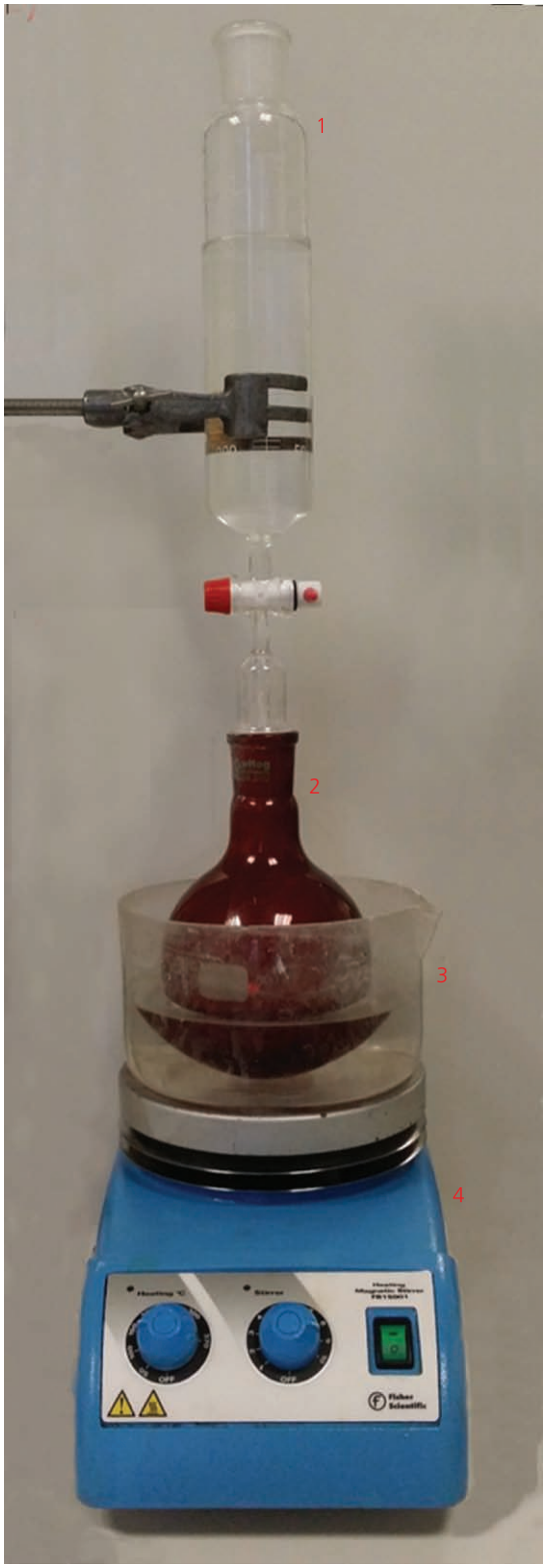

Figure 1. Sol–gel reaction system. 1, separator funnel containing 250 ml of a solution 7×10^{-4} M of cobalt (II) chloride (aq);[21] 2, round-bottomed flask containing 2-propanol and the titanium precursor; 3, crystalliser plate with water for the temperature bath; 4, hotplate/magnetic stirrer

flow into the reaction vessel at a rate of 2 ml/min. After continuous stirring for 6 h, a colloidal system with a concentration of 5 g/l cobalt-doped titanium dioxide was obtained through the reaction described in the following.

$$\text{I.}\quad Ti[OCH(CH_3)_2]_4 + 2H_2O \rightarrow TiO_2 + 4(CH_3)_2CHOH$$

The excess solvent was removed immediately after the completion of the reaction. The titanium dioxide was initially amorphous and required annealing to form the anatase crystalline phase that exhibits higher photocatalytic activity compared to amorphous or rutile titanium dioxide.[21] Annealing was carried out using an Elite BRF 14/10-2416 CG furnace with the material held in an alumina crucible with an internal volume of 20 ml. The annealing was achieved by ramping the temperature at a rate of 200°C/h, followed by a dwell at 450°C, for 2·5 h before cooling.

2.2 Application procedure for applying photocatalytic coating onto MDF

Water-based solutions were prepared containing 1% polyurethane (PU), 25% isopropyl alcohol (IPA) and 0·5% (0·02 g) titanium dioxide by weight. Rectangles with a surface area of 9 cm^2 were cut from the MDF wood board with a commercial paper decor finish impregnated with MUF. Approximately 0·25 ml of the selected solution was brushed onto the surface of the rectangular specimen, resulting in an estimated coating thickness of about 20 µm. The PU acted as the bonding agent to adhere the nanoparticles to the surface following evaporation of the water and IPA.

2.3 Compositional and morphological characterisations of photocatalytic coatings

X-ray diffraction (XRD) analysis was carried out to evaluate the percentage of crystalline amounts in the prepared specimens and microstructural features. Semi-quantitative analysis (quantitative phase analysis (QPA)) was attained by way of the Rietveld method on the XRD data. Rietveld refinements were assessed using the Gsas-EXPGUI software packages.[22,23] XRD data were collected on a Panalytical X'Pert Pro (NL) θ/θ diffractometer, using copper (Cu) Kα radiation (45 kV and 40 mA) with a step size of 0·02°2θ and time per step of 200 s over a 20–80°2θ range. The instrumental broadening was measured using the National Institute of Standards and Technology (NIST) SRM 660b standard[24] (LaB_6) – data collected under the same conditions as those used for the titanium dioxide samples. XRD was also used to determine microstructural features from the specimens. For this purpose, XRD data were collected in the same instrument with identical set-up as that used for QPA. A higher signal-to-noise ratio was achieved in the range of 20–115°2θ, using a step size of 0·1° and a time per step of 500 s. The instrumental contribution was obtained by parameterising the profile of 14 (hkl) reflections from the NIST SRM 660b standard (LaB_6), according to the Caglioti *et al.*[25] relationship. The microstructural features of the specimens were analysed by using the whole powder pattern modelling method,[26] as implemented in the PM2K software package. By means of this novel methodology, the size distribution of individual phases in nanoparticles can be accurately defined.[27] In this work, crystalline domains were assumed spherical and their diameter is distributed according to a log-normal curve. Raman spectra were acquired using a Renishaw System 2000 spectrometer equipped with an inVia Raman microscope using a helium (He)–neon (Ne) laser as an excitation source operating at 785 nm and a maximum power of 20 mW. The samples were analysed by focusing the laser with objective magnification of ×100 onto the sample surface corresponding to a laser spot diameter of about 10 µm. The acquisition time of 1 s was used for each spectrum over the wave number range of 100–1400 cm^{-1} with a 2 cm^{-1} resolution. The morphology of the aggregates and the composition of the cobalt-doped titanium dioxide and the surface of coated MDF boards was studied using a Jeol JSM-6480lv SEM with an Oxford Inca energy X-ray analyser correlated using an acceleration voltage of 20 keV and a spot size of 60 µm. A higher-magnification study of the particles was obtained using a Jeol FESEM6301F microscope with an acceleration voltage of 2 keV and a spot size of 5 µm.

2.4 Determination of photocatalytic activity of NPAs using methylene blue degradation test

The photocatalytic activity was evaluated at the liquid solid interface by monitoring the degradation of a methylene blue (MB) solution, containing the nanoparticles using an adaptation of the ISO 10678:2010 standard.[28] The solution was irradiated with UV light in the range of 375–385 nm with an average irradiation intensity of 15·44 W/m^2, visible green light in the range 525–535 nm with an average irradiation intensity of 12·32 W/m^2 and light-emitting diode white light with an average irradiation intensity of 16·74 W/m^2. All the light sources were situated 15 cm from the sample, and the intensities were measured using a Deltha Ohm photoradiometer HD 2102.1. The UV probe had a spectral range from 315 to 400 nm and an irradiance range from 0·1 mW/m^2 to 2000 W/m^2. The visible probe had a spectral range from 425 to 750 nm and a range of irradiance from 0·1 mW/m^2 to 2000 W/m^2. The degradation was monitored quantitatively with a Jenway 6300 spectrophotometer set at 670 nm using deionised water for calibration in a 1-cm-wide plastic cuvette. The initial absorbance of the MB solution was between 0·85 and 0·9 units depending on the sample. This value was recorded at the beginning of each experiment. To correlate the absorbance to the concentration, the Lambert–Beer law was applied in the following equation[28]

$$\text{1.}\quad A = \varepsilon_\lambda l C$$

where A is the absorbance; ε_λ is the molar absorption coefficient, typical for each compound and depending on the wavelength considered; l is the path length, in this case, it was the width of the cuvette; and C is the concentration of the dye.

For each sample, approximately 1 ml of a 1 M solution of MB was added to 100 ml of deionised water to obtain the appropriate

initial value of absorbance. Approximately 0·1 g of titanium dioxide was then added to these solutions. After a short period when the solution was stirred without irradiation, the first sample of solution for measurement was extracted using a 10-ml syringe and a filter unit (Sartorius Stedim, Minisart, 0·10 μm) to remove solid particles from the solution. After the first measurement, the light source was turned on to initiate the degradation reaction. A sample of the solution was taken at 5-min intervals, and a comparison is made between commercially available and synthesised particles with different light sources.

2.5 Determination of photocatalytic activity of coatings on MDF using Ink Intelligent dyes

The photocatalytic activity of the coatings on lime and wood were evaluated using Ink Intelligent dyes. Ink Intelligent is a spin-off company from Queen's University, Belfast, UK. The company has developed three different inks that provide a rapid and reliable method of evaluating the photocatalytic activity of a substrate. A semi-quantitative measure of the activity can be determined by evaluating the rate of colour change[29,30] during irradiation with UV light (375–385 nm) with an average irradiation value of 5·02 W/m^2 measured with a Deltha Ohm photoradiometer HD 2102.1 with a UV probe with spectral range from 315 to 400 nm and range of irradiance from 0·1 mW/m^2 to 2000 W/m^2. Different inks are available depending on the level of activity involved. In this study, the Explorer (Resazurin-based dye) was used for surfaces with medium activity and the Visualiser (Basic Blue 66-based dye) was used on surfaces with higher activity. Photocatalytic samples were tested alongside standard non-photocatalytic surfaces and, in all cases, half of the dye-coated-surface was covered with aluminium foil during irradiation. This allowed a comparison of colour change between photocatalytic and non-photocatalytic and irradiated and non-irradiated to be made.

3. Results and discussion

3.1 Characterisation of nanoparticle agglomerates

XRD patterns of titanium dioxide and cobalt–titanium dioxide specimens are shown in Figure 2; QPA data are reported in Table 1.

As shown in Table 1, the synthesised specimens contain the three most abundant titanium dioxide polymorphs. Unmodified titanium dioxide contains 67·7 wt% anatase, 3·9 wt% rutile and 28·4 wt% brookite. Cobalt–titanium dioxide is composed of 59·9 wt% anatase, 3·5 wt% rutile and 36·6 wt% brookite. The strong presence of brookite has to be ascribed to the acidic conditions

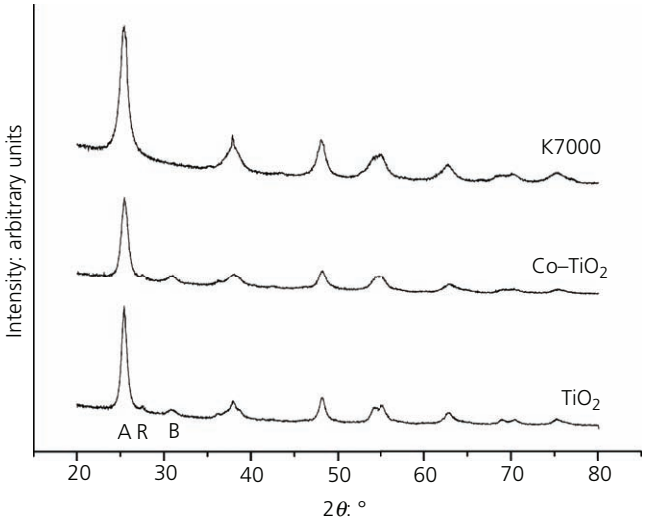

Figure 2. XRD patterns of synthesised and commercial specimens – A, R and B are symbols, standing for anatase, rutile and brookite, respectively

of the synthesis.[31] On the other hand, the presence of cobalt favoured the brookite crystallisation at the expense of anatase. While the cobalt-doped and undoped titanium dioxide contain the three polymorphs and no amorphous phase, the commercial Kronoclean 7000 consists of anatase with a low percentage of amorphous phase.

The microstructural features of the synthesised specimens are reported in Table 2. The primary average crystalline domain size of anatase in the commercial titanium dioxide specimen is 3·3 nm. The presence of cobalt in the synthesised sample increased this to 6·7 nm, as the anatase in the undoped titanium dioxide is 9·0 nm. As per rutile and brookite, their average crystalline domain sizes are, in undoped titanium dioxide, 7·6 and 8·9 nm and, in the cobalt-doped titanium dioxide, 12·4 and 8·6 nm.

Raman spectra were obtained to determine the crystalline structure of the samples, comparing the results with the literature. Figures 3 and 4 show the spectra for commercial and synthesised titanium dioxide.

In all the samples, the major crystalline structure was anatase, as indicated from the characteristic bands at 145, 197, 399, 516 and 640 cm^{-1}. In both doped and undoped synthesised samples, two

Table 1. Rietveld agreement factors and crystalline phase composition of the prepared specimens

Sample	Number of variables	Agreement factors			Phase composition: wt%			
		$R(F^2)$: %	R_{wp}: %	χ^2	Anatase	Rutile	Brookite	Amorphous
Kronoclean 7000	22	3·56	4·31	1·98	93·5 ± 1·1	0	0	6·5 ± 1·1
Titanium dioxide	22	2·33	4·14	1·45	67·7 ± 0·2	3·9 ± 0·2	28·4 ± 0·7	0
Cobalt–titanium dioxide	22	2·28	3·97	1·32	59·9 ± 0·2	3·5 ± 0·2	36·6 ± 0·7	0

Table 2. Mean crystalline domain diameter of Kronoclean 7000, undoped titanium dioxide and cobalt–titanium dioxide

Sample	Mean crystalline domain diameter		
	D_{ant}: nm	D_{rt}: nm	D_{brk}: nm
Kronoclean 7000	3·3 ± 0·1	0	0
Titanium dioxide	9·0 ± 0·9	7·6 ± 0·4	8·9 ± 0·4
Cobalt–titanium dioxide	6·7 ± 0·6	12·4 ± 2·6	8·6 ± 0·3

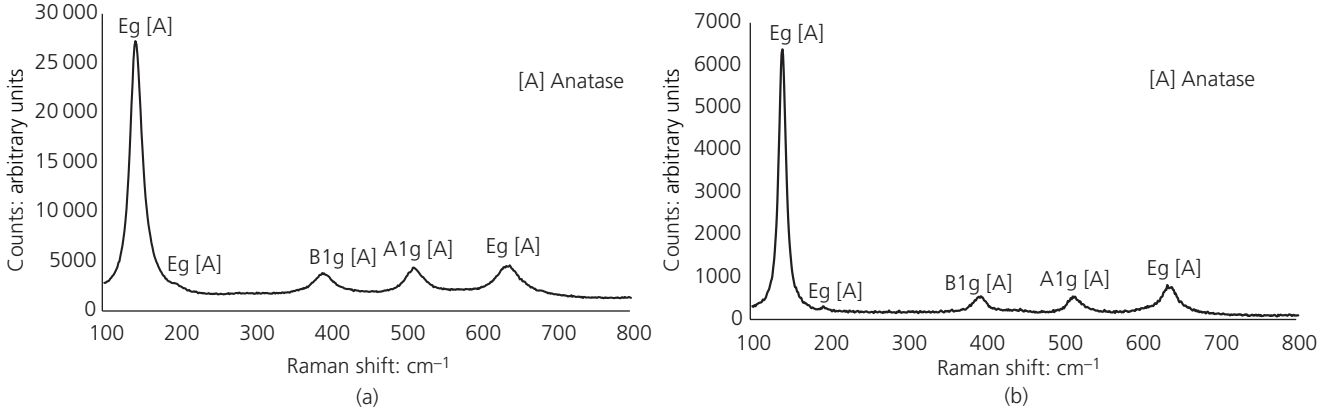

Figure 3. (a) Raman spectrum of Kronoclean 7000[32] and (b) Raman spectrum of Degussa P25[33]

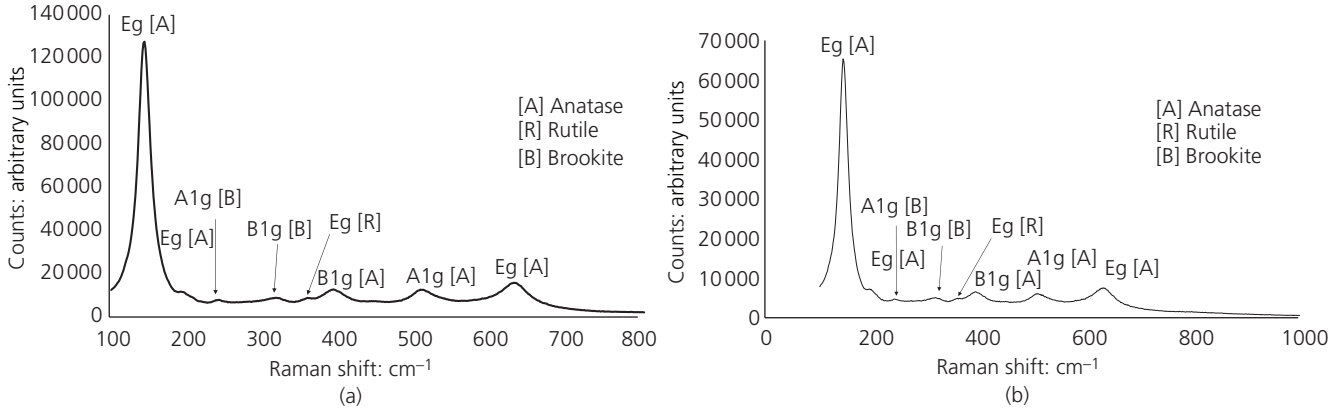

Figure 4. (a) Raman spectrum of cobalt-doped titanium dioxide annealed at 450°C for 2·5 h and (b) Raman spectrum of undoped titanium dioxide annealed at 450°C for 2·5 h

additional phases are present where bands at 244 and 330 cm^{-1} are attributed to residual rutile and where the bands at 250 and 322 cm^{-1} are assigned to brookite phase in the samples following annealing.

Raman and XRD data confirm the presence of the three polymorphs. The morphology at different magnifications was studied using SEM and FESEM. During the thermal treatment, sintering is evident between the nanoparticles which led to the formation of aggregates. Figures 4(a) and 4(b) show a large aggregate of nanoparticles around 100 µm wide, together with smaller aggregates, from 1–30 µm wide. All the aggregates are formed from individual nanoparticles, as shown in Figures 5(a) and 5(b). The nanoparticles have an average dimension of 47 nm (±5 nm); the distances were measured using image-processing software on post-processing analysis.

Figure 6 shows the morphology of the MDF substrate at the microscale when coated with cobalt-doped titanium dioxide. As described previously, the MDF is finished with an MUF-coated paper to give a white appearance and aesthetically pleasing finish. This white coating, however, contains a proportion of rutile

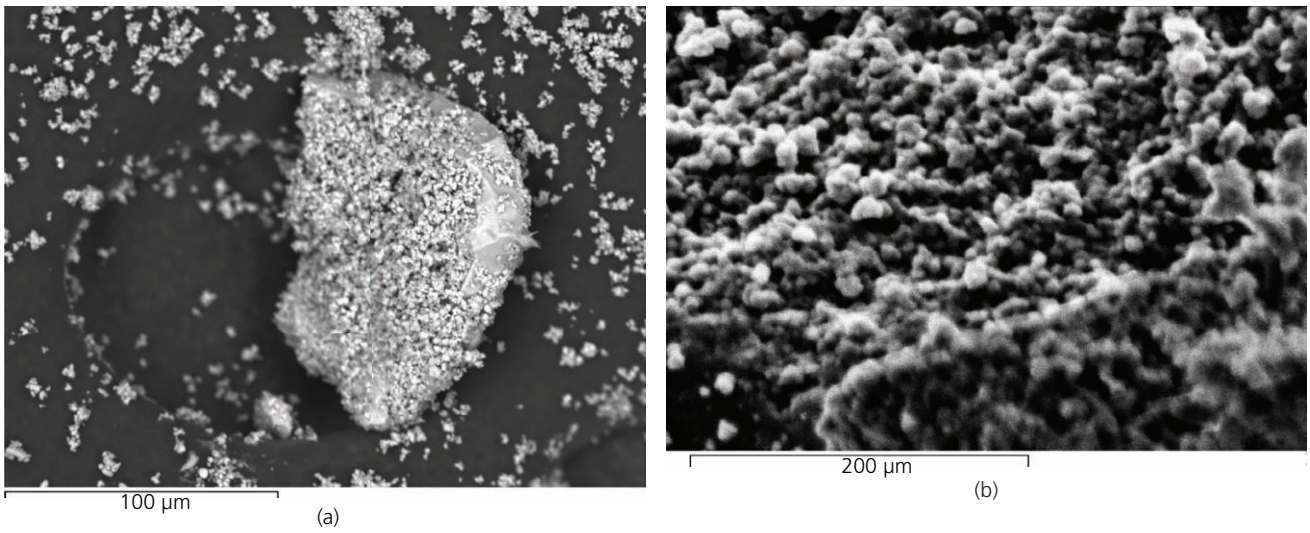

Figure 5. (a) SEM image of cobalt-doped titanium dioxide annealed at 450°C with a magnification of ×400 and (b) SEM image of the surface of titanium dioxide cobalt-doped aggregate annealed at 450°C with a magnification of ×3500

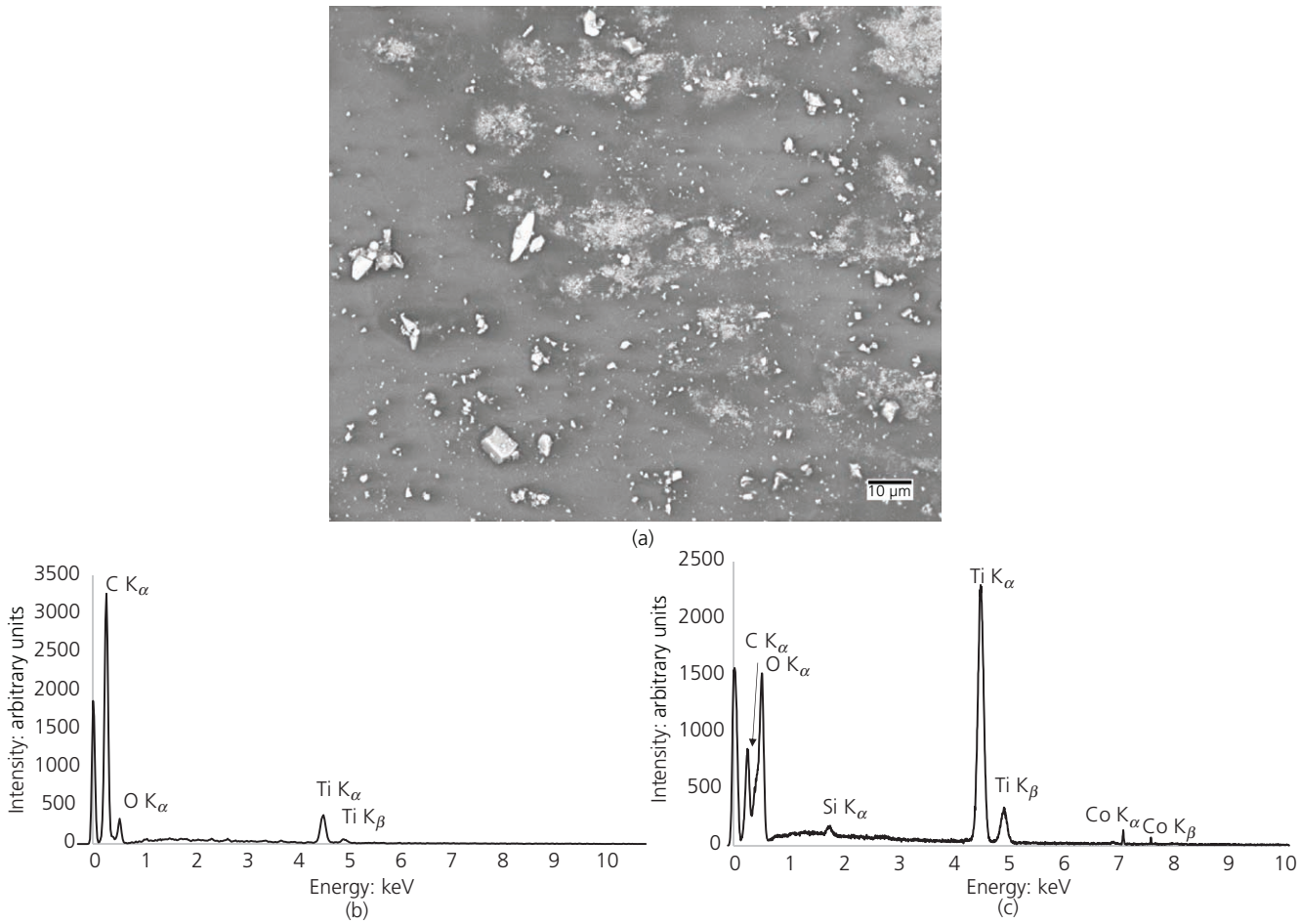

Figure 6. (a) SEM image of MDF coated with cobalt-doped titanium dioxide, (b) EDX spectra on MUF resin (containing rutile–titanium dioxide pigment) and (c) EDX on titanium dioxide aggregate

titanium dioxide which is employed as a pigment. The cobalt-doped titanium dioxide aggregates of nanoparticles are evident as particles on the surface. Due to their porous structure and low conductivity, some surface charging under the electron beam is evident, and these are clearly visible. The darker background, the grey area, is attributed to the paper coating. When analysed using EDX analysis, the spectrum shown in Figure 7(b) is obtained. Peaks corresponding to carbon, oxygen and titanium are visible

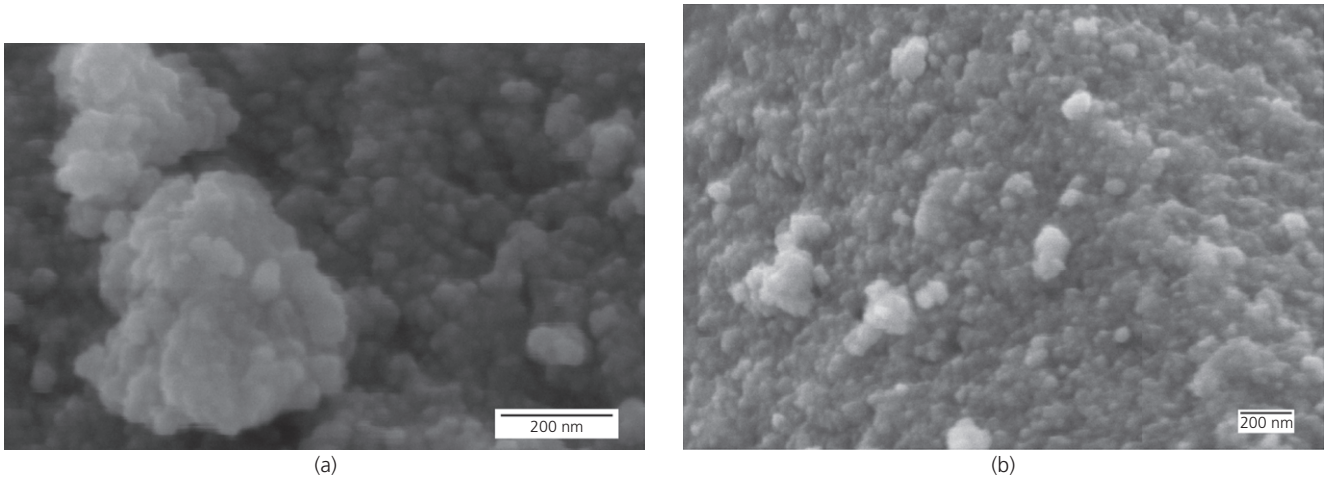

Figure 7. (a) FESEM image of aggregated cobalt-doped titanium dioxide particles with a magnification of ×120 000 and (b) FESEM image showing nanostructures of undoped titanium dioxide particles with a magnification of ×100 000

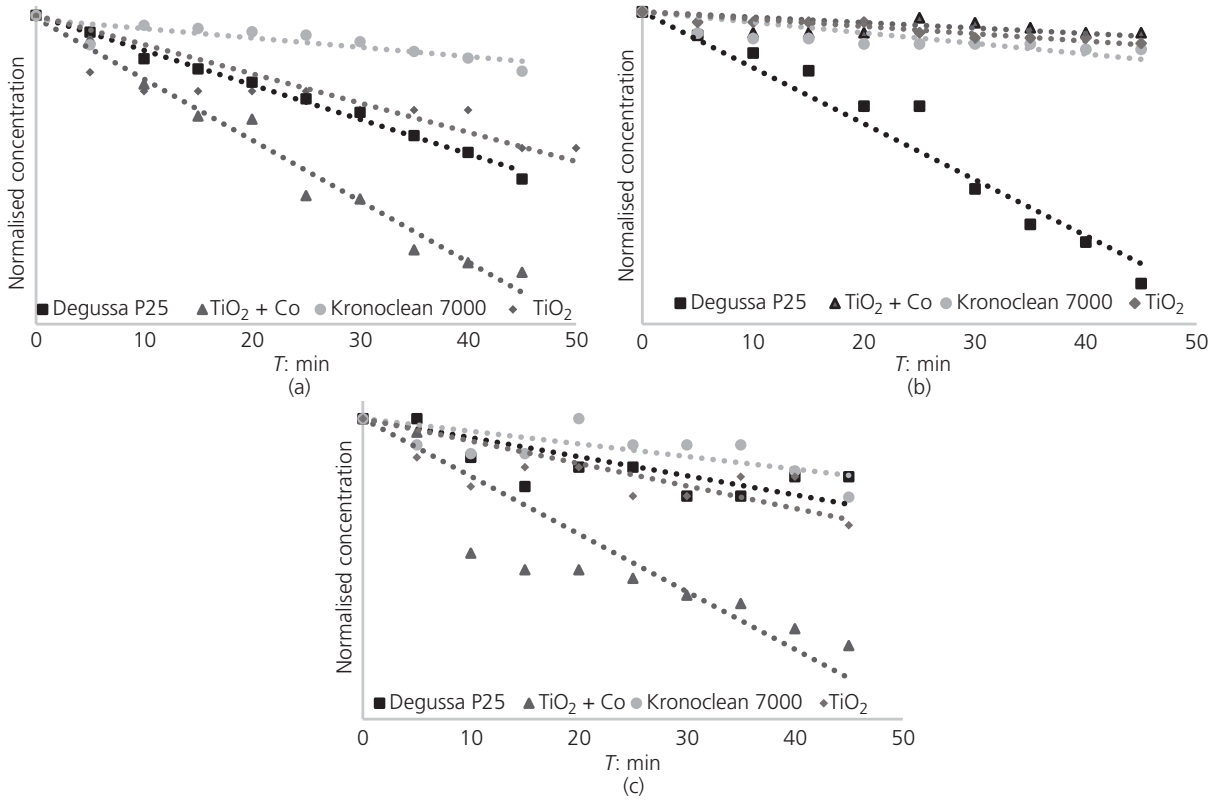

Figure 8. Degradation of MB solution in the presence of nanoparticles, (a) irradiated with UV light, (b) irradiated with green light and (c) irradiated with white light

with the titanium signal originating from the rutile pigment. The analysis of the cobalt-doped titanium dioxide gives a similar spectrum. Due to the sensitivity of the EDX analysis and the relatively low cobalt-doping concentration, 1%, peaks corresponding to cobalt are not evident within the spectrum of a single point, but a larger area was scanned to obtain the peaks of interest.

3.2 Evaluation of photocatalytic activity using degradation of MB

The degradation of a solution of MB was carried out to confirm and measure the photocatalytic activity of the particles considering the reactions at the liquid–solid interface. Figures 6(a)–6(c) show the normalised concentration against time in solutions irradiated with lights of different wavelength.

Degradation under UV light in Figure 8(a) demonstrates the superior performance of commercially available Degussa P25 compared to Kronoclean 7000 and undoped and cobalt-doped titanium dioxide. When irradiated with green light (Figure 8(b)), the performance of the synthesised doped titanium dioxide is comparable with the P25, and pure titanium dioxide is slightly less active; furthermore, broadening the irradiation wavelength with white light enhances this effect. Figure 8(c) shows that the performance of undoped titanium dioxide is comparable with the P25, whereas the doped sample showed the best performance under visible light, confirming that doping with cobalt enhances the photocatalytic activity in the range examined.

3.3 Photocatalytic activity detection with Ink Intelligent inks

Ink Intelligent inks were used as a qualitative method to confirm the photocatalytic activity of the particles once applied onto the surfaces of wood-based materials. During the irradiation period, half of the samples were coated to compare the degradation due to the photocatalytic activity and oxidation reactions.

Figure 9 presents typical results from three different coatings; the indicator stripes on the left and right are BB66 and Rz, respectively. The presence of the coating on the surface modified the wettability of the substrate which is apparent from the non-uniformed application of the Rz-based ink. The bottom half of the substrates (below the dashed line) was shielded with a metal plate. The photocatalytic activity was correlated to the change in colour from blue to pink and then transparent in the BB66-based ink and from blue to transparent in the Rz-based ink. The synthesised cobalt-doped material displays a more intense reaction, with the inks showing a faster degradation compared to undoped and commercial particles. In all cases, the degradation begins 5 min after the initial irradiation.

4. Conclusions

Cobalt-doped titanium dioxide NPAs were successfully synthesised using a sol–gel process involving the reaction of titanium tetraisopropoxide at 80°C. Nanoparticles with a mean diameter of 47 nm (±5 nm) were produced. The experimental

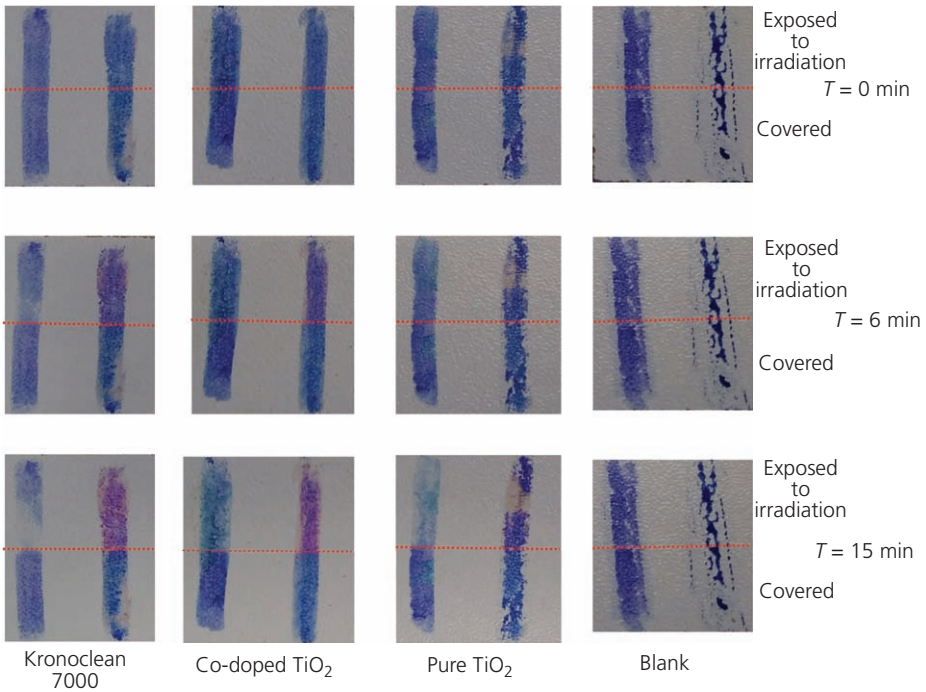

Figure 9. Ink Intelligent photocatalytic test on MDF samples coated with Kronoclean 7000, cobalt-doped titanium dioxide, pure titanium dioxide and blank irradiated with UV light. BB66-based ink applied on the left side of the MDF samples changes colour from blue to colourless, and Rz on the right side changes colour from blue to pink

conditions employed in this study produced the three polymorphs of titanium dioxide in the nanoparticles. These polymorphs differ from commercial particles, which are constituted of anatase and a small proportion of amorphous material, indicated by XRD and Raman spectra. The presence of cobalt in the lattice promoted the formation of the brookite polymorph and caused a colouration of the titanium dioxide powder from white (in the case of pure titanium dioxide) to a brown–yellow colour.

The degradation of MB by the cobalt-doped titanium dioxide was observed under UV radiation (375–385 nm), green light (525–535 nm) and white light (5200 K). P25 showed the best performance under the UV light. When the degradation was studied using light in the visible range, cobalt-doped titanium dioxide was more photocatalytically active than commercial, undoped titanium dioxide. Photosensitive organic inks (Ink Intelligent) were employed to evaluate the photocatalytic activity of polymer coatings applied to decor finishes on MDF substrates. Photocatalytic activity was observed in all the materials incorporating titanium dioxide nanoparticles. The superior catalytic performance of the cobalt-doped titanium dioxide compared to the best commercial pure titanium dioxide Degussa P25 and carbon-doped titanium dioxide Kronoclean 7000 in the range of visible light indicates promise for future research and further applications in indoor air environments.

Acknowledgements

The research leading to these results has received funding from EU's Seventh Framework Programme (FP7/2007-2013) under grant agreement 609234. The authors also acknowledge support from Kronospan, UK, for supplying the MDF substrates, and from Kronos, for supplying the titanium dioxide nanoparticles.

REFERENCES

1. Fujishima A, Honda A and Iwata K (1972) Electrochemical photolysis of water at a semiconductor electrode. *Nature* **238(5358)**: 37–38, http://dx.doi.org/10.1038/238037a0.
2. Fujishima A, Zhang X and Trykc DA (2008) TiO_2 photocatalysis and related surface phenomena. *Surface Science Reports* **63(12)**: 515–582.
3. Paz Y (2010) Application of TiO_2 photocatalysis for air treatment: patents' overview. *Applied Catalysis B: Environmental* **99(3–4)**: 448–460.
4. Long R and English NJ (2011) Band gap engineering of double-cation-impurity-doped anatase–titania for visible-light photocatalysts: a hybrid density functional theory approach. *Physical Chemistry Chemical Physics* **13(30)**: 13698–13703.
5. Litter M (1999) Heterogeneous photocatalysis transition metal ions in photocatalytic systems. *Applied Catalysis B: Environmental* **23(2–3)**: 89–114.
6. Cheng XW, Yu XJ, Xing ZP and Wan JF (2012) Enhanced photocatalytic activity of nitrogen doped TiO_2 anatase nano-particle under simulated sunlight irradiation. *Energy Procedia* **16(Part A)**: 598–605, http://dx.doi.org/10.1016/j.egypro.2012.01.096.
7. Nuño M, Pesce GL, Bowen CR, Xenophontos P and Ball RJ (2015) Environmental performance of nano-structured $Ca(OH)_2/TiO_2$ photocatalytic coatings for buildings. *Building and Environment* **92**: 734–742, http://dx.doi.org/10.1016/j.buildenv.2015.05.028.
8. Nuño M, Ball RJ, Bowen CR, Kurchania R and Sharma GD (2015) Photocatalytic activity of electrophoretically deposited (EPD) TiO_2 coatings. *Journal of Materials Science* **50(14)**: 4822–4835.
9. Nuño M, Ball RJ and Bowen CR (2014) Study of solid/gas phase photocatalytic reactions by electron ionization mass spectrometry. *Journal of Mass Spectrometry* **49(8)**: 716–726.
10. Ferreira Pinto Da Silva CF, Maskell D, Ball R and Ansell M (2014) The physical, chemical and mechanical properties of eco-materials for passive indoor environmental control. In *Advanced Building Skins – Conference Proceedings of the 9th Energy Forum*. Economic Forum, Munich, Germany, pp. 367–380.
11. Maskell D, da Silva CF, Mower K *et al.* (2015) Properties of bio-based insulation materials and their potential impact on indoor air quality. *First International Conference on Bio-based Building Materials, Clermont-Ferrand, France.*
12. Won D, Corsi RL and Rynes M (2001) Sorptive interactions between VOCs and indoor materials. *Indoor Air* **11(4)**: 246–256.
13. Da Silva CFFP, Rana C, Maskell D *et al.* (2016) Influence of eco-materials on indoor air quality. *Green Materials* **4(2)**: 72–80, http://dx.doi.org/10.1680/jgrma.16.00002.
14. Redlich A, Sparer J and Cullen MR (1997) Sick-building syndrome. *The Lancet* **349(9057)**: 1013–1016.
15. Han G, Umemara K, Zhang M, Honda T and Kawai S (2001) Development of high-performance UF-bonded reed and wheat straw medium-density fiberboard. *Journal of Wood Science* **47(5)**: 350–355.
16. Woodson GE (1976) Effects of bark, density profile, and resin content on medium-density fiberboards from southern hardwoods. *Forest Products Journal* **26(2)**: 39–42.
17. Ye XP, Julson J, Kuo M, Womac A and Myers D (2007) Properties of medium density fiberboards made from renewable biomass. *Bioresource Technology* **98(5)**: 1077–1084.
18. Baumann MGD, Lorenz LF, Batterman SA and Zhang GZ (2000) Aldehyde emissions from particleboard and medium density fiberboard products. *Forest Products Journal* **50(9)**: 75–82.
19. Giampiccolo A, Ball RJ and Ansell MP (2014) Synthesis of Co-doped TiO_2 nanostructures for novel photo-catalytic coatings. In *Advanced Building Skins – Conference Proceedings of the 9th Energy Forum*. Economic Forum, Munich, Germany, pp. 997–1007.
20. O'Regan B and Gratzel M (1991) A low cost, high efficiency solar cell based on dye-sensitized colloidal TiO_2 films. *Nature* **353(6346)**: 737–740, http://dx.doi.org/10.1038/353737a0.
21. Sclafani A and Herrmann JM (1996) Comparison of the photoelectronic and photocatalytic activities of various anatase and rutile forms of titania in pure liquid organic phases and in aqueous solutions. *Journal of Physical Chemistry* **100(32)**: 13655–13661, http://dx.doi.org/10.1021/jp9533584.
22. Larson AC and Von Dreele RB (2000) *General Structure Analysis System (GSAS)*. Los Alamos National Laboratory, Los Alamos, NM, USA.
23. Toby BH (2001) EXPGUI, a graphical user interface for GSAS. *Journal of Applied Crystallography* **34(2)**: 210–213.
24. Black DR, Windover D, Hennis A, Filliben J and Cline JP (n.d.) *Standard Reference Material 660B for X-ray Metrology*. National Institute of Standards and Technology, Gaithersburg, MD, USA. See http://www.icdd.com/resources/axa/vol54/V54_17.pdf (accessed 24/11/2016).
25. Caglioti G, Paoletti A and Ricci FP (1960) On resolution and luminosity of a neutron diffraction spectrometer for single crystal analysis. *Nuclear Instruments and Methods* **9(2)**: 195–198.
26. Leoni M, Confente T and Scardi P (2006) PM2K: a flexible program implementing whole powder pattern modelling. *Zeitschrift für Kristallographie Supplemente* **23**: 249–254.
27. Mittemeijer EJ and Scardi P (2004) *Diffraction Analysis of the Microstructure of Materials*. Springer, Dordrecht, the Netherlands.
28. ISO (International Organization for Standardization) (2010) ISO 10678:2010: Fine ceramics (advanced ceramics, advanced technical ceramics) – determination of photocatalytic activity of surfaces in an

aqueous medium by degradation of methylene blue. ISO, Geneva, Switzerland.
29. Mills A, Hepburn J, Hazafy D *et al.* (2013) A simple, inexpensive method for the rapid testing of the photocatalytic activity of self-cleaning surfaces. *Journal of Photochemistry and Photobiology A: Chemistry* **272**: 18–20, http://dx.doi.org/10.1016/j.jphotochem.2013.08.004.
30. Mills A and McGrady M (2008) A study of new photocatalyst indicator inks. *Journal of Photochemistry and Photobiology A: Chemistry* **193(2–3)**: 228–236.
31. Hu Y, Tsai HL and Huang CL (2003) Effect of brookite phase on the anatase–rutile transition in titania nanoparticles. *Journal of the European Ceramic Society* **23(5)**: 691–696.
32. Tobaldi DM, Seabra MP, Otero-Irurueta G *et al.* (2015) Quantitative XRD characterisation and gas-phase photocatalytic activity testing for visible-light (indoor applications) of KRONOClean 7000®. *RSC Advances* **5(124)**: 102911–102918.
33. Choi HC, Jung YM and Kim SB (2005) Size effects in the Raman spectra of TiO_2 nanoparticles. *Vibrational Spectroscopy* **37(1)**: 33–38.